IV.A.1 Efficient Discovery of Novel Multicomponent Mixtures for Hydrogen Storage: A Combined Computational/Experimental Approach

Prof. Christopher Wolverton (Primary Contact),
Prof. Vidvuds Ozolins[1], Prof. Harold H. Kung,
Dr. Jun Yang[2]
Department of Materials Science & Engineering
Northwestern University
Evanston, IL 60208
Phone: (847) 467-0593
Email: c-wolverton@northwestern.edu
[1]University of California, Los Angeles
[2]Ford Motor Company

DOE Managers
HQ: Ned Stetson
Phone: (202) 586-9995
Email: Ned.Stetson@ee.doe.gov
GO: Katie Randolph
Phone: (720) 356-1759
Email: Katie.Randolph@go.doe.gov

Contract Number: DE-FC36-08GO18136

Project Start Date: September 1, 2008
Project End Date: July 31, 2013

Fiscal Year (FY) 2012 Objectives

The objective of this project is to discover novel mixed hydrides for hydrogen storage, which enable the DOE 2010 system-level goals. Our goal is to find a material that desorbs 8.5 wt% H_2 or more at temperatures below 85°C. The research will combine first-principles calculations of reaction thermodynamics and kinetics with material and catalyst synthesis, testing, and characterization. We will combine materials from distinct categories to form novel multicomponent reactions. Examples of systems to be studied include mixtures of complex hydrides and chemical hydrides and novel multicomponent complex hydride materials and reactions.

Technical Barriers

This project addresses the following technical barriers from the Storage section of the Fuel Cell Technologies Program Multi-Year Research, Development and Demonstration Plan:

(P) Lack of Understanding of Hydrogen Physisorption and Chemisorption

(A) System Weight and Volume

(E) Charging/Discharging Rates

Technical Targets

This study is aimed at fundamental insights into new materials and the thermodynamic and kinetic aspects of hydrogen release and reabsorption from them. Insights gained from these studies will be applied toward the design and synthesis of hydrogen storage materials that meet the following DOE 2010 hydrogen storage targets:

- Specific energy: 1.5 kWh/kg
- Energy density: 0.9 kWh/L

FY 2012 Accomplishments

- H_2 desorption and decomposition pathways have been studied in
  - $5LiBH_4 + 2Mg(BH_4)_2$ (~5.8 wt% desorbed)
  - $Mg(BH_4)_2 + Mg(NH_2)_2$ (~8.3 wt% desorbed)
  - $(NH_4)_2B_{12}H_{12}$. (~4.5 wt% desorbed)
- Partial reversibility (~1-2.5 wt%) found in $5LiBH_4 + 2Mg(BH_4)_2$ and $(NH_4)_2B_{12}H_{12}$
- Proposed new metal-carbon catalyst: Tested on $NaAlH_4$, and applied to $Mg(BH_4)_2 + Mg(NH_2)_2$, $2LiBH_4+5Mg(BH_4)_2$ and $LiBH_4$; effective catalyst - lowers desorption temperature, improves dehydrogenation rate, and suppresses formation of borane and NH_3
- Down-select the mixed borohydride/amide systems as promising hydrogen storage material (lack of reversibility and B-N bonds in products)
- Predicted a new metastable $Mg_3(B_3H_6)_2$ intermediate in decomposition of $Mg(BH_4)_2$, but showed that recently-proposed $Mg(B_3H_8)_2$ is not stable.
- Prototype electrostatic ground state plus density functional theory combined experimental measurements are used in unique way to solve amorphous AlB_4H_{11} polymeric structure (with J.C. Zhao, Ohio State University)
- Using the predictive models of defects, kinetics of mass transport: mass transport in $LiBH_4$ is very low (much lower than that in $NaAlH_4$)

❖   ❖   ❖   ❖   ❖

Introduction

The long-term DOE targets for hydrogen storage systems are very challenging, and cannot be met with existing materials. The vast majority of the work to date has delineated materials into various classes, e.g., complex and metal hydrides, chemical hydrides, and sorbents. However, very recent studies indicate that mixtures of storage materials, particularly mixtures between various classes, hold promise to achieve technological attributes that materials within an individual class cannot reach. Our project involves a systematic, rational approach to designing novel multicomponent mixtures of materials with fast hydrogenation/dehydrogenation kinetics and favorable thermodynamics using a combination of state-of-the-art scientific computing and experimentation. Specifically, we focus on combinations of materials from distinct categories to form novel multicomponent reactions.

Approach

We use the accurate predictive power of first-principles modeling to understand the thermodynamic and microscopic kinetic processes involved in hydrogen release and uptake and to design new material/catalyst systems with improved properties. Detailed characterization and atomic-scale catalysis experiments elucidate the effect of dopants and nanoscale catalysts in achieving fast kinetics and reversibility. And, state-of-the-art storage experiments give key storage attributes of the investigated reactions, validate computational predictions, and help guide and improve computational methods. In sum, our approach involves a powerful blend of: 1) H_2 storage measurements and characterization, 2) state-of-the-art computational modeling, 3) detailed catalysis experiments, and 4) an in-depth automotive perspective.

Results (Selected Examples)

I. High-resolution desorption data for the following three prioritized mixtures: $(NH_4)_2(B_{12}H_{12})$, $2LiBH_4 + 5Mg(BH_4)_2$, and $Mg(NH2)_2 + Mg(BH_4)_2$

Our recent experimental efforts focused on obtaining high-resolution desorption and recharging data as well as phase identification for the following three prioritized mixtures: $(NH_4)_2(B_{12}H_{12})$, $2LiBH_4 + 5Mg(BH_4)_2$, and $Mg(NH2)_2 + Mg(BH_4)_2$. Building off of the temperature-programmed desorption mass spectrometry (TPDMS) data previously obtained, we focused on phase identification via in situ X-ray diffraction (XRD) and Fourier transform infrared (FTIR) experiments as well as water displacement desorption (WDD) to establish reversibility. The XRD measurements were performed in a flowing nitrogen (200 sccm) environment using a sapphire substrate with a temperature

ramp of 1°C/min from 50 to 550°C after a 1-hour room-temperature scan. For the variable temperature scans, each scan was integrated for 10 minutes, providing averaged data over a 10°C window. Phases were identified using the MDI JADE software package and the ICDD Powder Diffraction Database. For the FTIR experiments, both diffuse reflectance infrared Fourier transform spectroscopy (DRIFTS) and photo acoustic (PAS) FTIR methods were used. DRIFTS measurements allowed us to explore local environment changes with changes in temperature. The samples to be measured via DRIFTS were contained in a sample holder under flowing argon. The chamber containing the sample holder was purged with nitrogen and the sample temperature ramped at a rate of 5°C/min from room temperature to 450°C. Every minute, 16 sample scans were collected during the temperature ramp and a powdered KBr background was used. For the PAS measurements, the sample holder was purged with helium while the enclosure was purged with nitrogen. All PAS measurements were taken at room temperature, with a carbon black background and collected 32 sample scans for each spectrum. Because of the different WDD conditions used, the details of the measurements are only given in the relevant section below.

1. **$2LiBH_4 + 5Mg(BH_4)_2$**: The $LiBH_4/Mg(BH_4)_2$ mixture was prepared by ball milling as-purchased $LiBH_4$ and $Mg(BH_4)_2$ in a 2:5 molar ratio. Our XRD measurements (Figure 1) revealed that the mixture resembled a physical mixture of $LiBH_4$ and $Mg(BH_4)_2$, though the peaks corresponding to LiBH4 were partially convoluted with the substrate. The measurements revealed several steps of decomposition: 1) consumption of $LiBH_4$ and partial consumption of $Mg(BH_4)_2$(decreasing intensity of peaks) between 200-250°C, 2) full consumption of $Mg(BH_4)_2$ and possible MgB_2 or MgH_2 formation (250-300°C), and 3) above 350°C, the formation of MgB_2, and the formation of peaks corresponding to an unidentified phase (at $2\theta = \sim30\text{-}40°$). This reaction path differs from that predicted by thermodynamics, which we attribute to kinetic limitations in the system. This conclusion is supported by the difference in observed desorption onset versus the predicted temperature (approximately 200°C vs. -29° C).

    We used WDD to examine the reversibility of this mixture, as well. The experiment was performed by ramping the sample from room temperature to 350°C at 5°C/min and holding for approximately 2 hours. To recharge the system, the temperature was maintained and the sample exposed to 138 bar ultra-high purity (UHP) hydrogen for approximately 18 hours. The process was then repeated for each cycle. We found indications of limited reversibility under the conditions used (Figure 2).

2. **$Mg(NH2)_2 + Mg(BH_4)_2$**: The $Mg(NH_2)_2/Mg(BH_4)_2$ mixture was produced by ball milling as-purchased $Mg(BH_4)_2$ with $Mg(NH_2)_2$ synthesized from
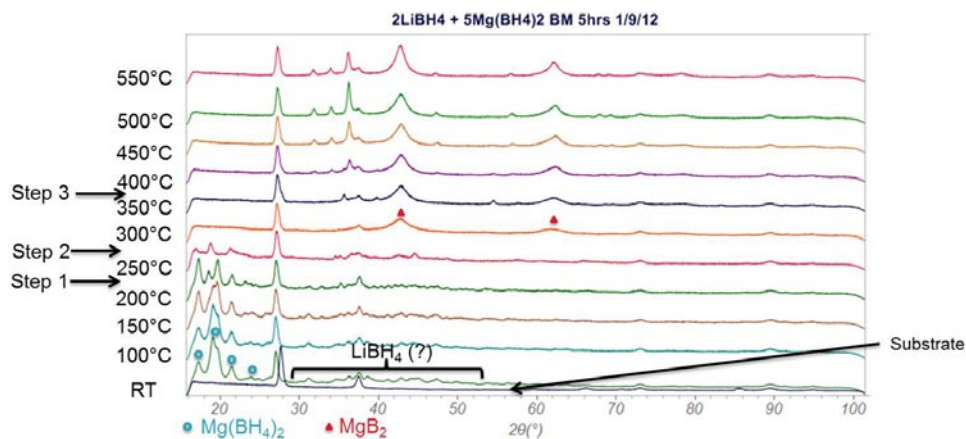
FIGURE 1. XRD measurements of ball milled $2LiBH_4+5Mg(BH_4)_2$

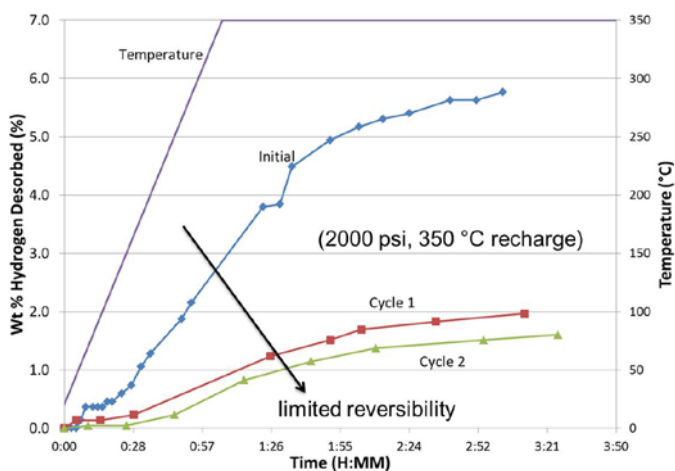**FIGURE 2.** Reversibility studies of mixed $2LiBH_4+5Mg(BH_4)_2$
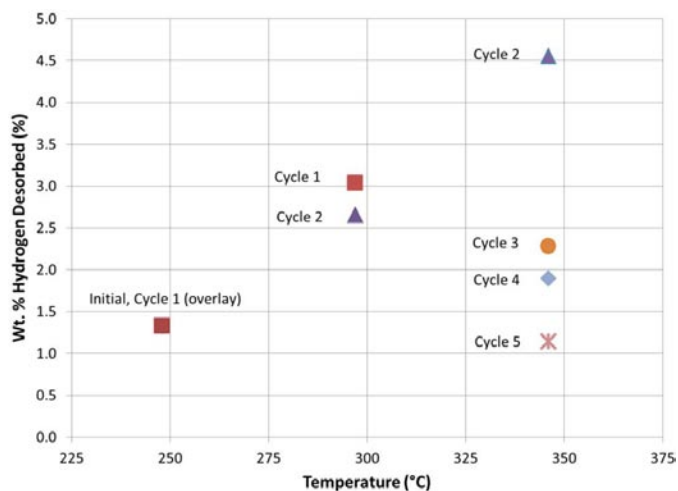
FIGURE 3. Partial reversibility of $(NH_4)_2B_{12}H_{12}$

MgH_2 and 20 bar NH_3. Like the $LiBH_4/Mg(BH_4)_2$ mixture, we reported previously that the onset of hydrogen desorption occurs at ~200°C, a significantly lower temperature than the pristine constituents, with a second hydrogen release event at roughly 400°C. Northwestern and Ford collaborated closely in the identification of the reaction products and pathway, with Ford providing available XRD and infrared data to assist in the determination of reaction products via computational methods, including PEGS to determine new structures. However, further study of the system via WDD found it to be irreversible under the conditions tested: 1) ramp to 250°C at 5°C/min, cool to room temperature for recharge with 114 bar UHP hydrogen, 2) ramp to 380°C at 5°C/min, maintain for recharge with 138 bar UHP hydrogen.

3. **$(NH_4)_2(B_{12}H_{12})$**: This compound was synthesized and kindly provided to Ford by J.C. Zhao (Ohio State University). We reported previously that hydrogen

desorption begins at roughly 250°C, and occurs in two primary steps. Our TPDMS results indicated that little NH_3 is released and undetectable quantities of diborane or borazine are produced during decomposition. We found evidence of partial reversibility up to 350°C via WDD cycling experiments (Figure 3). The WDD experiment was carried out as follows:

–   Initial desorption to 250°C at 5°C/min and holding for approximately two hours.

–   Recharge overnight at the above temperature with 138 bar UHP hydrogen.

–   Cool sample to room temperature, purge excess hydrogen from the system.

–   Ramp sample to 250°C at 5°C/min and hold for two hours (Cycle 1, 250°C in (Figure 3).

–   After the two hours at 250°C, the sample was ramped up to 300°C at 5°C/min and held (Cycle 1, 300°C in Figure 3).

- Recharge overnight at 300°C under 138 bar UHP hydrogen.
- Repeat process for subsequent temperatures.

II. Characterizing carbon/Ni catalysts for LiBH$_4$ dehydrogenation

The effect of carbon on the dehydrogenation kinetics of LiBH$_4$. In view of the observed favorable dehydrogenation and hydrogenation kinetics of carbon-based catalysts on NaAlH$_4$, we initiated the study of carbon and Ni/carbon catalysts on the dehydrogenation of LiBH$_4$ and the results are shown in Figure 4. The dashed curves are the dehydrogenation profiles of physical mixtures of LiBH$_4$ mixed with carbon containing 2% Ni; which was loaded on using the precursor bis(cyclooctadiene)nickel(0). The weight loading of LiBH$_4$ in the physical mixture of LiBH$_4$ and Ni containing carbon was 47% and 68% respectively for curve **a** and curve **c**. For curve **b**, the loading of LiBH$_4$ in the mixture was 48% but the carbon contained no Ni. Curve **d** is the profile for 100% LiBH$_4$ and shows that dehydrogenation kinetics was very sluggish;similar to what was reported in the literature. The data clearly show that the dehydrogenation kinetics were enhanced with increasing carbon content in the physical mixture and for a given ratio of carbon and LiBH$_4$ (compare black dash and pink solid curves), the presence of Ni mildly enhanced the dehydrogenation rate.

LiBH$_4$-carbon-Ni composite synthesized with a one-step infusion. Since it appears that the contact between carbon and LiBH$_4$ is important, we explored ways to increase the contact area between LiBH$_4$ and carbon in the mixture. Figure 5 shows the data for a composite sample where the LiBH$_4$ is in more intimate contact with the carbon than just that of a physical mixture. The curve labeled Composite is for a sample, containing 70 wt% LiBH$_4$, that
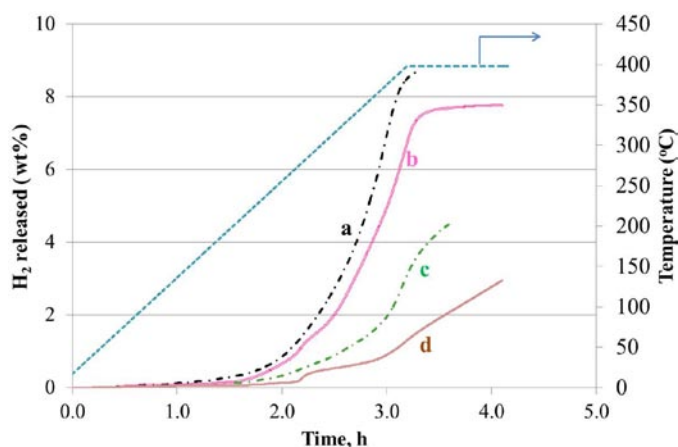
was made by mixing a tetrahydrofuran (THF) solution of bis(cyclooctadiene)nickel(0) and LiBH$_4$ with carbon (Norit, SX Ultra Cat). The THF solvent was removed by evacuation at room temperature for an extended time period and then by an additional 25 min evacuation at 60°C. Compared with a physical mixture, the composite began decomposing at a substantially lower temperature. Although we have yet to firmly establish that hydrogen release was the cause for the increase in pressure in the reactor, particularly at low temperatures, the low boiling point of THF (66°C) and the fact that we had previously established effective THF removal by room temperature evacuation of a THF solution containing bis(cyclooctadiene)nickel(0) and Norit carbon, led us to believe that at least some of the pressure increase was due to hydrogen evolution.

LiBH$_4$-Y carbon composite made by multi-step infusion (Composite C1 and C2). In order to further enhance the contact between LiBH$_4$ and carbon, we modified the preparation procedure of the composite by using a multiple impregnation technique. In this technique, the total volume of LiBH$_4$ in THF solution was divided into small portions, and each portion was dried onto the carbon consecutively. In this way, most of the solution would be in the pores of the carbon, such that selective deposition on the external surface of the carbon is minimized.

For these composites, a higher surface area carbon material was used, which was a carbon molecular sieve (Y carbon; Inc) with a surface area of 3,200 m^2/g. Its surface area is even higher than a single graphene sheet (2,630 m^2/g), possibly due to the presence of defects. For these samples, the LiBH$_4$ was introduced using the glass apparatus shown in Figure 6, which afforded addition of a THF-LiBH$_4$ solution to carbon in dry nitrogen; and drying by evacuation without
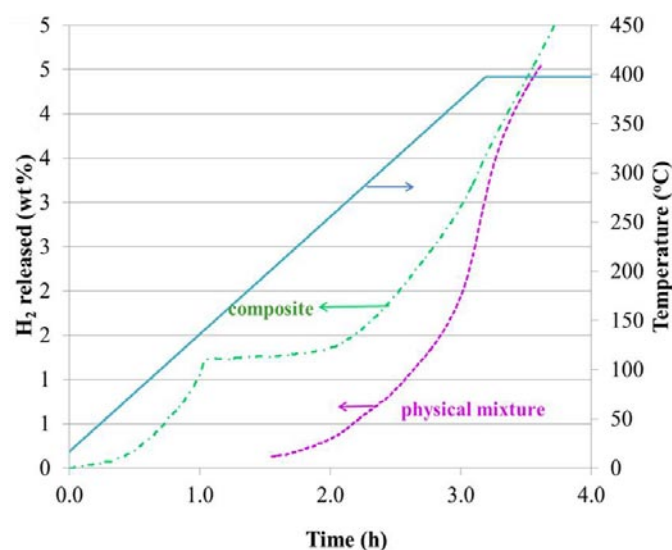

FIGURE 4. Dehydrogenation profile of carbon (Norit SX Ultra Cat) and LiBH$_4$ physical mixture; (a) 47% LiBH$_4$ and 53% carbon containing 2% Ni, (b) 48% LiBH$_4$ and 52% carbon, (c) 68% LiBH$_4$ and 32% carbon containing 2% Ni, and (d) 48% LiBH$_4$.

FIGURE 5. Comparison of the dehydrogenation kinetics of a physical mixture and a composite of Norit carbon and LiBH$_4$.

FIGURE 6. Synthesis glassware

FIGURE 7. Comparison of the dehydrogenation of composite C1 (LiBH$_4$ infused into Y carbon) and a physical mixture of Norit carbon and LiBH$_4$
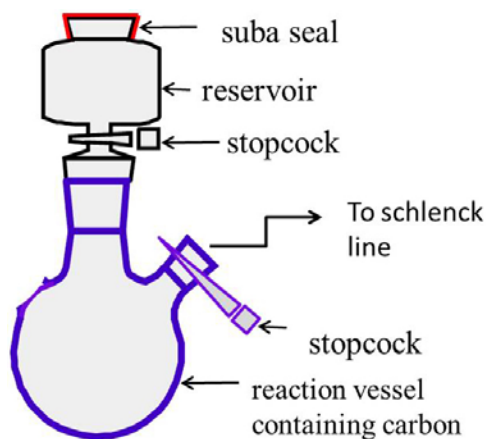
the need to transfer the sample. Aliquots of the THF-LiBH$_4$ solution, enough to fill the pore volume of the carbon, was introduced into the reservoir using a syringe pump, and then dripped into the reaction vessel, all without exposure to air. Then the solvent was removed by evacuation at around 40°C. After drying, another aliquot was introduced and the procedure was repeated until the desired amount of LiBH$_4$ was added (about 30 wt%).

The decomposition profile of this sample (labeled composite C1) is shown in Figure 7. Because of some uncertainties of the amount of LiBH$_4$ added, due to splashing of the LiBH$_4$ solution onto the reactor wall, the Y axis is labeled as approximate H$_2$ released. The dehydrogenation kinetics was enhanced significantly for this sample than a physical mixture of carbon and LiBH$_4$. Very interestingly, low temperature H$_2$ release was observed.

This experiment was repeated with an improved procedure that reduced splashing of the LiBH$_4$ onto the wall of the reaction vessel, and composite C2 was prepared. The decomposition profile of this sample is shown in Figure 8a.

A series of dehydrogenation and rehydrogenation experiments was conducted using composite C2 and the temperature sequence of these operations is shown in the scheme depicted in Figure 8b. The black solid lines denote the hydrogenation portion of the experiment, and the dehydrogenation portions are denoted by the dashed lines. Different colored curves of the data in Figure 8a and 8c correspond to the dehydrogenation steps of the same color depicted in Figure 8b. Figure 8c is the magnified low-temperature portions of the data in Figure 8a.

When the composite C2 was first heated with a temperature ramp of 2°C/min to 250°C and maintained at that temperature for 5 min (curve I), a low-temperature H$_2$ release was observed similar to that seen for composite C1, indicating that the synthesis of the composites is repeatable. When the sample at this point was rehydrogenated at 240°C
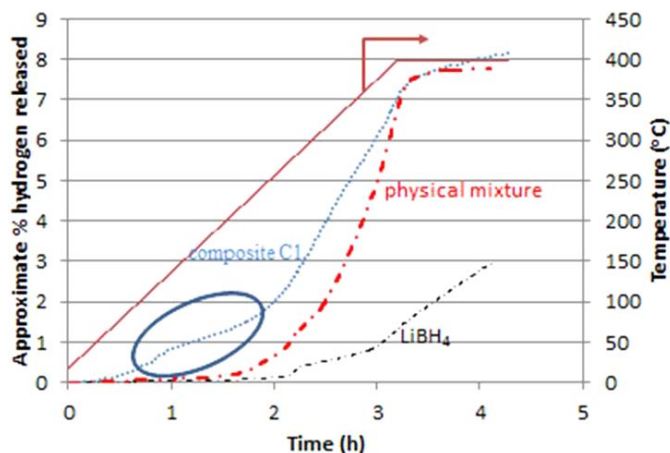
with 12.8 bar H$_2$, subsequent dehydrogenation experiment showed a very low but detectable level of H$_2$ release (curve II, Figure 8a and Figure 8c). At this point, the sample was cooled to room temperature and dehydrogenation was conducted again at 2°C/min ramp to 400°C and the sample was kept at 400°C for 37 min (curve III). Little H$_2$ release was observed below 200°C but the rate of release was accelerated above 250°C. The total H$_2$ release from the three dehydrogenation experiments was 10.2 wt% of LiBH$_4$. The dehydrogenated sample was rehydrogenated at 13.8 bar and 390°C for 0.5 h and cooled down to room temperature and evacuated. The dehydrogenation profile of this rehydrogenated sample is shown in curve IV (Figures 8a and 8c). There was still some H$_2$ released below 200°C but the amount was very small. The total H$_2$ released for the rehydrogenated sample was 2.5%. Since the pressure of the rehydrogenation experiment was very low, it is not clear whether the sample had picked up the maximum amount of H$_2$. When the hydrogenation was repeated with a slightly higher pressure of 15.3 bar at 390°C, the dehydrogenation profile obtained was similar (curve V of Figure 8a and 8c). he uptake of hydrogen during rehydrogenation was fast. At this point, we believe that more extensive rehydrogenation can be obtained using a much higher H$_2$ pressure.

The dehydrogenation and rehydrogenation results using the composite of carbon-LiBH$_4$ are promising but the current synthesis procedure is cumbersome. We plan to investigate alternate, easier methods to form these composite with the same or better hydrogen storage properties. In addition, addition of Ni and Pd will be explored to enhance low temperature dehydrogenation kinetics.

III. Mass transport in lithium borohydride

LiBH$_4$ has a high volumetric and gravimetric (18.4 wt%) hydrogen density and has shown partial reversibility, but the kinetics remain very slow at temperatures below
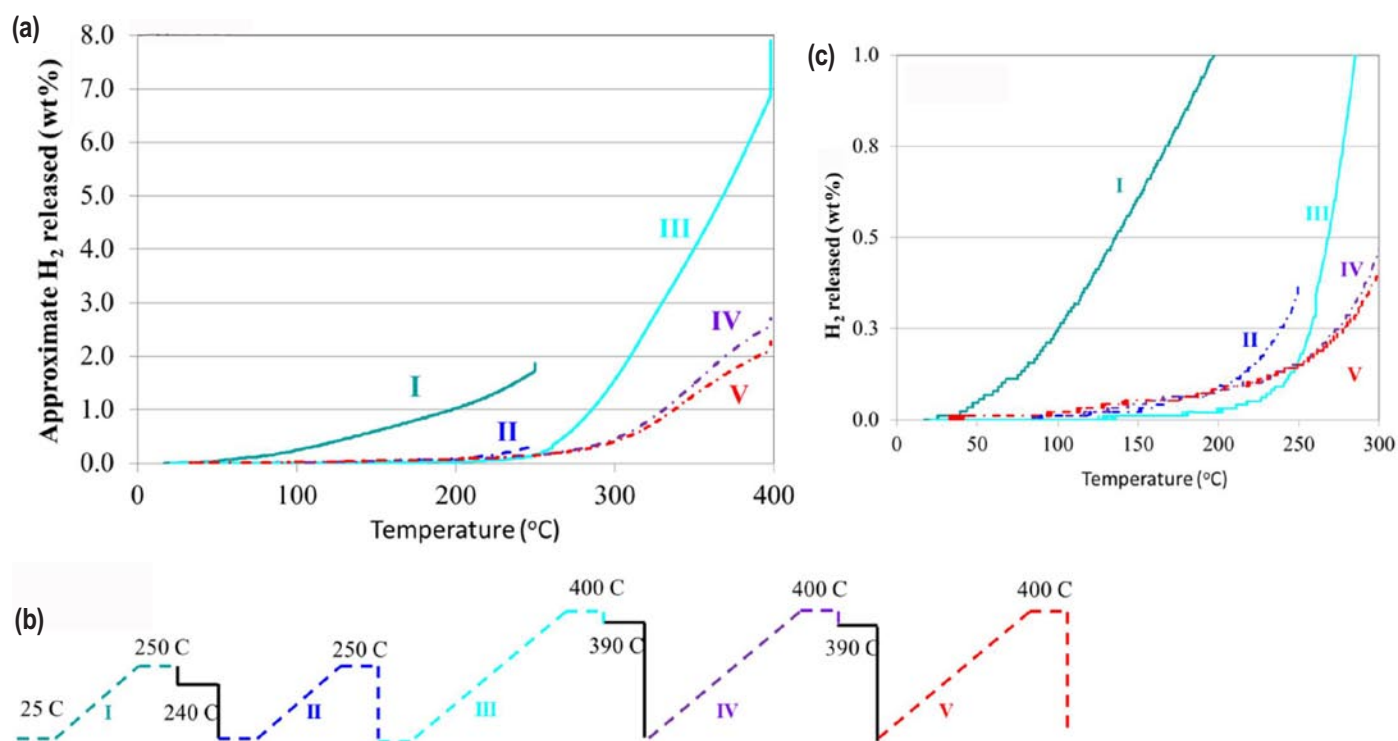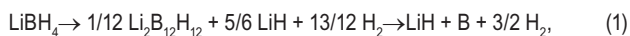
FIGURE 8. Dehydrogenation and hydrogenation of composite C2

its melting point of approximately 280°C. Even though the thermodynamic properties of pure LiBH$_4$ are not suitable for onboard storage, we have predicted several destabilized reactions involving LiBH$_4$ with equilibrium reaction temperatures below the melting point of LiBH$_4$. Thermodynamically, these reactions are allowed at temperatures compatible with proton exchange membrane fuel cells, but almost all of them are inhibited kinetically and require melting of the reactants to show appreciable hydrogen release rates. It is natural to hypothesize that slow rates of mass transport in the solid state is a key reason for the slow hydrogen release kinetics in solid. Hence, understanding of the kinetics of solid-state mass transport could provide clues for developing effective catalytic doping strategies.

Thermodynamically, the solid-state dehydrogenation reaction is predicted to occur in the following two-step process:

$$\text{LiBH}_4 \rightarrow 1/12\ \text{Li}_2\text{B}_{12}\text{H}_{12} + 5/6\ \text{LiH} + 13/12\ \text{H}_2 \rightarrow \text{LiH} + \text{B} + 3/2\ \text{H}_2, \quad (1)$$

Our calculation shows that the total reaction enthalpy is $\Delta H = 83$ kJ/(mol H$_2$) at T=0 K, in line with the experimentally determined value of $\Delta H = 74$ kJ/(mol H$_2$). The calculated enthalpies of the first-step and second-step reactions are 61 and 141 kJ/(mol H$_2$), respectively.

We have completed a systematic study of mass transport in solid LiBH$_4$ and its decomposition products, Li$_2$B$_{12}$H$_{12}$ and

LiH, using the mass transport model recently developed by us. This formalism is based on local equilibrium assumptions at interfaces where diffusion is driven by concentration gradients across the phases participating in Reaction (1). Defect formation energies are calculated from the density-functional theory, and both charged and neutral defects are taken into account. Chemical potentials are set by local equilibrium assumptions at the interfaces shown in Figure 9, and lead to nonzero mass fluxes through the participating phases.

Our results show that defects with the highest concentration in the products LiH and Li$_2$B$_{12}$H$_{12}$ are compensating intrinsic defect pairs, the creation of which does not involve exchange of atoms with any of the coexisting phases in Reaction (1). Hence, their concentration is uniform throughout the sample and they have zero concentration gradients and negligible mass fluxes. In LiH, the dominant defects are Schottky pairs of [H]$^+$ and [Li]$^-$ vacancies, while in Li$_2$B$_{12}$H$_{12}$ they are Frenkel pairs of Li$^+$ interstitials and [Li]$^-$ vacancies. In the reactant LiBH$_4$, negatively charged Li vacancies ([Li]$^-$), positively charged Li interstitials (Li$^+$), positively charged BH$_4$ vacancies [BH$_4$]$^+$, and neutral BH$_3$ vacancies [BH$_3$] have the highest concentrations. Among them, only the neutral [BH$_3$] vacancies have an appreciable concentration gradient, while the others are mutually compensating intrinsic defects with small gradients (see Figure 10).
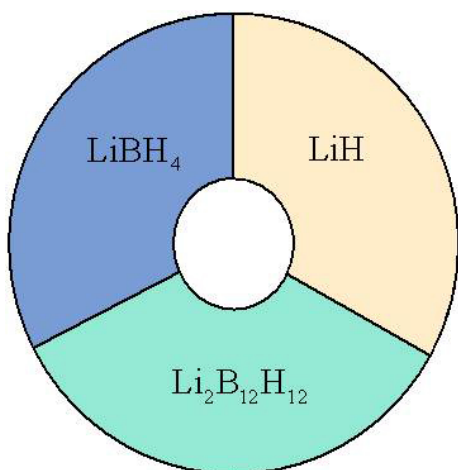
FIGURE 9. Schematic reaction morphology for reaction (1) showing the possible interfaces, which in turn determine the mass fluxes through the reactant and product phases
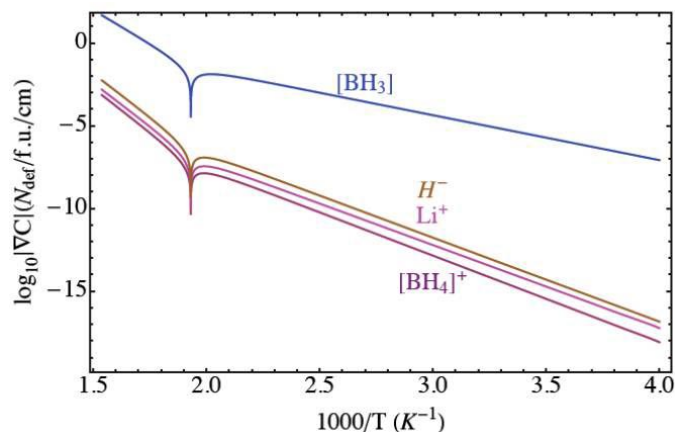

FIGURE 11. Structure of the neutral [BH$_3$] vacancy in LiBH$_4$. The H- anion is shown as red, Li+ cations are dark green, B atoms are blue, and H atoms are pink. Red dashed lines indicate that the H- anion is tetrahedrally coordinated with the surrounding Li+ cations.

FIGURE 10. The calculated concentration gradients in LiBH$_4$

Future Directions

- Experimentally characterize storage properties/reactions of $(NH_4)_2B_{12}H_{12}$ and other predicted reactions; Optimize reversibility conditions for $5Mg(BH_4)_2+2LiBH_4$ mixture.

- Extend experimental catalyst studies to other predicted promising materials; explore optimal morphology of carbon/metal catalysts.

- Focus experimental efforts on rehydriding reactions/reversibility (subject to pressure limitations of experimental equipment).

- Focus computational efforts on kinetics, defects, diffusion/mass transport/hydrogen dissociation in promising predicted reactions.

- Down-select decision: End work on borohydride/amide combinations. (No reversibility from computational or experimental work; B-N bonds in product.)

The structure of the neutral [BH$_3$] vacancy is shown in Figure 11. It shows that removing a BH$_3$ complex leaves behind a negatively charged H$^-$ anion occupying the vacant site. Compared with the [AlH$_3$] vacancy diffusion mechanism in NaAlH$_4$, the [BH$_3$] vacancy diffusion in LiBH$_4$ is blocked by the negative H$^-$ anion left behind after creating the [BH$_3$] vacancy. We conclude that mass transport in solid LiBH$_4$ is very slow and likely represents a key rate-limiting process of the dehydrogenation reaction based on this material. In the future studies, we plan to investigate catalytic strategies for accelerating diffusion by either using reactants with faster rates of mass transport or by doping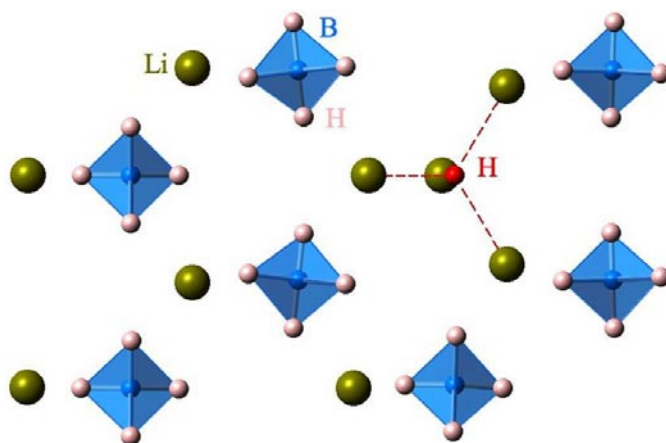 with elements to create additional anion vacancies.